Technical Sciences
Academy of Romania
www.jesi.astr.ro

Journal of Engineering Sciences and Innovation
Volume 8, Issue 2 / 2023, pp. 101– 112

A. Mechanical Engineering

Received ***26 January 2023*** *Accepted* ***26 June 2023***
Received in revised form ***28 Apryl 2023***

Coating of a lignin-based polymer with ceramic micro-powders

ALINA MARGUTA[1], SIMONA-NICOLETA MAZURCHEVICI[1]
DUMITRU NEDELCU[1,2*]

[1]Department of Machine, Manufacturing Technology,
"Gheorghe Asachi" Technical University of Iasi, 700050 Iasi, Romania;
[2]Mechanical Engineering Department, Technical Sciences Academy of Romania,
030167 Bucharest, Romania

Abstract. This paper examines the behavior of Arboblend V2 Nature biopolymer samples coated with three distinct ceramic powders: Amdry 6420 (Cr_2O_3), Metco 143 (ZrO_2 $18TiO_2$ $10Y_2O_3$), and Metco 136F (Cr_2O_3-$xSiO_2$-$yTiO_2$). Atmospheric Plasma Spray (APS) method were used to deposit the coating onto the polymeric substrate, which was obtained by injection molding. Several characteristics of the coated samples, as thermal behavior, roughness, as well as structural and morphological aspects, were evaluated during the investigation. The surface analysis of the samples demonstrated a uniform deposition for the ZrO_2 $18TiO_3$ $10Y_2O_3$ layer, but a less uniform deposition for the coatings containing ceramic micro-particles of chromium (III) oxides. The thermal research revealed the material's structural resilience. Regarding Atomic Force Microscopy examination, it highlighted the roughness of the coated surfaces and also the good adhesion of the micro-particles on the biopolymer substrate.

Keywords: coating, biodegradable thermoplastic, micro-powders, characterization.

1. Introduction

In order to decrease surface degradation and increase the thermal resistance of polymer surfaces, the researchers devised a viable solution involving the application-specific application of ceramic or metallic microlayers. In order to

*Correspondence address: dnedelcu@tuiasi.ro

improve resistance to wear, corrosion, oxidation, and heat, [1–4], ceramic coatings have been widely used in a variety of applications.
The best-known methods for coating polymeric surfaces are TS - thermal spray as APS, PVD (physical vapour deposition), metal plating, and CVD - chemical vapor deposition [5-10]. According to the variables implicated in the coating process, it is expected that each of these methods will have both advantages and disadvantages.
Atmospheric plasma spray (APS) is a popular thermal deposition method, and coatings made from ceramic layer depositions are frequently used in mechanical applications, [11]. The main problems with these coatings are the micro-cracks, isolation inhomogeneity, and residual stresses (which develop during the cooling process), [12].
Summary of factors influencing thermal spray processing of polymer, [13, 14]:
- Torch variable: power, type of thermal energy, gas composition, temperature, cooling;
- Jet variable: jet exit velocity and temperature, particle velocity and temperature, particle trajectory;
- Spraying distance;
- Feedstock variable: power type, powder size, and shape, carrier gas – flow and velocity, injection geometry;
- Particle variable: impact energy, impact angle, solidification state, rheology, morphology;
- Post-treatments – coatings;
- Cooling mechanism;- Pre-treatments:powder, substrate;
- Substrate variable: substrate type, substrate temperature.
In the literature, coatings are mostly about how well they protect against corrosion [15]; smart coatings are able to stabilize some features like thermal stability, resistance to scratching and strong chemical acids, high optical transmission etc., [16]; corrosion resistance and electrical conductivity, [17]; anticorrosion durability, [18]; anticorrosive coatings in the marine field, coating failure and adhesion loss, [19].
The goal of the manuscript was to find a new material with better properties that could be used instead of synthetic plastics in the auto industry.

2. Materials and methods

Arboblend V2 Nature, a lignin-based polymer, was chosen to be coated with ceramic microparticles. This one is biodegradable, its matrix taken from annual vegetable plants or from the waste of the paper industry, as stated by the manufacturers and corroborated by several studies in the specialized literature [20-22]. Polylactic acid (PLA - also biodegradable polyester) and other biodegradable elements and a limited amount of natural additives (resins, waxes, shellac) can also be found in the Arboblend V2 Nature structure [23-25].
The sample to be coated was made by injecting it into a mold with the SZ-600H machine. Its dimensions were 70 x 50 x 10 mm3. For injection, the following

technical parameters were used: the melting point of the material was 165°C, the injection pressure was 100 MPa, the injection speed was 80 m/min, and the cooling time was 30 seconds. With the help of SPRAYWIZARD-9MCE equipment, the injected samples were coated using atmospheric plasma spray (APS) technology. The gun used was a 9MB, the spray distance was between 137 and 145 mm, and the powder amount was between 126 and 144 g/min, the air pressure was 1.4 Bar, the carrier gas flow (NLPM) was between 5.1 and 5.3, and the rate of micro-particle deposition was constant.

Three ceramic powders (bought from the manufacturer Oerlikon Metco) with the following trade names and chemical composition were utilized for the coating, [26]:

- Amdry 6420 - Chromium Oxide Thermal Spray Powder (Cr_2O_3), angular shape, blocky morphology, (10–105) µm;
- Metco 136F - Chromia–Silica composite powder (Cr_2O_3-xSiO_2-yTiO_2), irregular or angular/ blocky morphology, (9–110) µm, Cr_2O_3 - Balance; SiO_2 - (3.0 - 4.5) %; TiO_2 < 4.0 %;
- Metco 143 - Zirconia–Titania–Yttria Composite Powder (ZrO_2 18TiO_2 10Y_2O_3), spheroidal morphology; typically, particle size between (3–40) µm.

Three samples injected with Arboblend V2 Nature were coated with the three micro-powders. Seven passes were performed on each sample in order to observe the effect of the deposited ceramic layer on the sample's properties.

To analyze the surface topography and roughness of the coated samples, an AFM (Atomic Force Microscopy) examination was conducted using the Nanosurf easyScan 2 equipment, which also includes the Nanosurf EasyScan 2 data representation software. The area examined was roughly (49.5 x 49.5) μm^2.

On a DSC 200 F3 Maia differential scanning calorimeter (NETZSCH-Geratebau GmbH, Selb, Germany), differential scanning calorimetry (DSC) was conducted. The device was calibrated in line with standards for mercury (Hg), zinc (Zn), indium (In), tin (Sn), and bismuth (Bi). Les samples tested had a mass of less than 30 mg. Experiments were examined in an inert gas atmosphere (Ar). A sample and a reference (an empty crucible) were treated to the identical temperature program in this experiment. The temperature program involved heating from room temperature (20 °C) to 200 °C and then cooling again to 20 °C. The utilized heating and cooling rate was 10 K/min. Throughout the experiment, the reference and sample temperatures were measured, and the temperature difference was transformed into heat flux.

The QUANTA 200 3D electron microscope was utilized for scanning electron microscopy (SEM) (FEI Company, Fremont, CA, USA). On the surface of the samples coated with ceramic micro-powders, micrographic maps were created to observe primarily the uniformity of the deposition. The primary factors considered were as follows: microscope chamber pressure - 60 Pa; the detector is a Large Field Detector for the analysis of non-conductive samples such as polymers, textile fibers, and powders; the tilt angle is 0°; the secondary electron acceleration voltage is 20 Kv; the working distance is 15 mm; and the magnification range is 500 and

2000 for details. To determine the chemical elements that appeared with the deposition of the ceramic layers, an X-ray diffraction analysis (XRD) was conducted using the X'Pert Pro MRD X-ray diffractometer, which has a Cu kα anode X-ray tube, λ–1.54, Panalytical equipment and a voltage of 45 kV, with the diffraction angle 2θ. Two X'Pert Data Collector programs, X'Pert High Score Plus version 3 and X'Pert Data Viewer version 2.2 g, were used to process the data and generate the diagrams. This investigation sought to determine the occurrence of crystallization phases unique to ceramic micro-powders placed on the surface of Arboblend V2 Nature samples. The crystallization phases were identified by comparing the obtained data to those found in the research literature.
The chemical composition analyses were conducted at five unique locations, and Minitab software was used to calculate the average composition.

3. Results and discussion

3.1. DSC Analyse

The DSC study was done just on the sample coated with ZrO_2 $18TiO_3$ $10Y_2O_3$ to determine if thermal spraying affects the structure of the substrate due to the ceramic layer. Figure 1 depicts the sample compartment during calorimetric analysis, and Table 1 details the transformations that occur. In addition, the earlier thermal testing of the samples [23, 27] were considered.
When heated, the sample exhibited three distinct transformations—two endothermic (I^{st} and III^{rd}) and one exothermic (II^{nd}). This thermal behavior was also observed in the Arboblend V2 Nature sample that was not coated with a ceramic micro-layer, [21, 22].
Below are the temperatures at which each of these three changes occurs: The initial temperature is denoted by T_{onset}, the intermediate temperature by T_{peak}, the final temperature by T_{end} (calculated by the tangent method), and the total heat released or absorbed by a given mass, DH/m (using a rectilinear baseline).

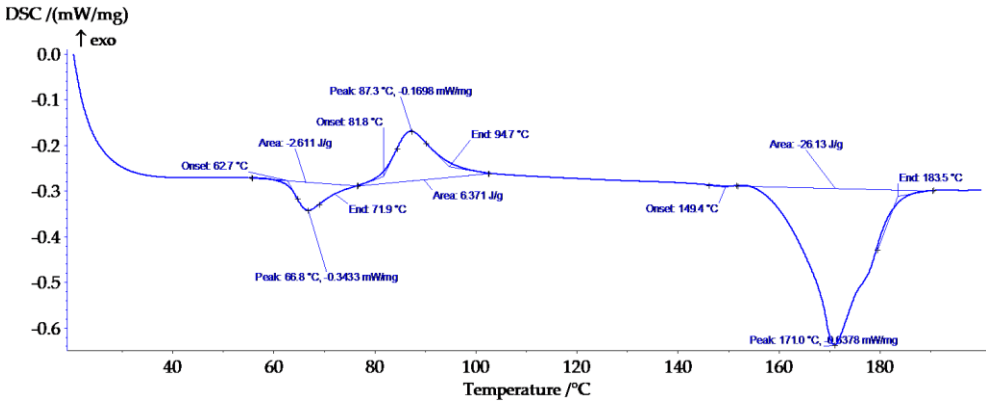

Fig. 1. The thermal behaviors of the tested sample,
Arboblend V2 Nature + ZrO_2 $18TiO_3$ $10Y_2O_3$.

By looking at the initial phase change, it is shown that the samples reach an endothermic maximum around 66.8°C, which is linked to a slow monotropic transformation of the solid-solid type and of some metastable crystals, [28], which occurs with less heat being absorbed per unit mass.
The second peak occurs at about 87 °C; this exothermic peak is linked to either the crystallization of the biopolymer's fundamental matrix, lignin, or the reticular rearrangement of lignin, [29].
Significant heat absorption (22.13 kJ/kg) occurs at the third peak. Arboblend V2 Nature biopolymer melting at 171°C is responsible for the endothermic transition.

Table 1. Calorimetric characterization of sample coated with ceramic layer

Sample	**Transformation**	**T_{onset} [°C]**	**T_{peak} [°C]**	**T_{end} [°C]**	**ΔH/m [kJ / kg]**
Arboblend V2 Nature coated with ZrO_2 $18TiO_3$ $10Y_2O_3$	**I**	62.7	66.8	71.9	-2.61
	II	81.8	87.3	94.7	6.37
	III	149.4	171	183.5	-26.13

3.2. SEM Analysis

Figure 2(a) depicts the morphology of Arboblend V2 Natural material coated with Metco 143. (ZrO_2 $18TiO_2$ $10Y_2O_3$). A homogeneous covering is found on the biopolymer substrate. The coating comprises of spherical component particles that retain their shape as a result of extremely quick cooling upon contact with the polymeric substrate. Also, it can be noticed that the substrate comprises a variety of particles in shape and size (3–40) μm, [26], in high quantities and in an even distribution, which leads to an improvement in mechanical qualities.
Figure 2(b) illustrates the polymer matrix including particles from the chromium oxide-formed coating. Some of these particles are scattered heterogeneously, while others are embedded inside the polymeric structure. The particles have the unique rectangular form of chromium oxide. The spherical micro-particles can be linked to the existence of Fe_2O_3 and SiO_2, which are discharged in modest amounts from the Amdry 6420 powder's structure, no more than 0.4% and 0.45%, respectively. Compared to the sample coated with Metco 143, the material included a smaller quantity of powder appearance, indicating a poorer capability for coating and embedding chromium oxide into the polymeric structure.
Similar to Figure 2(b), the coating of chromium oxide, silicon oxide, and titanium oxide (Cr_2O_3-$xSiO_2$-$yTiO_2$, Figure 2(c)) reveals a rather uneven distribution of micro-particles. There are several particle forms, including polyhedral (TiO_2), spherical (SiO_2), and rectangular (Cr_2O_3). Incorporating the particles into the polymer bulk. Figures 2(b) and (c) both depict chromium oxide, which does not exhibit superior adherence in comparison to the sample coated with ZrO_2 $18TiO_2$ $10Y_2O_3$ (Figure 2(a)), which does not include chromium oxide.

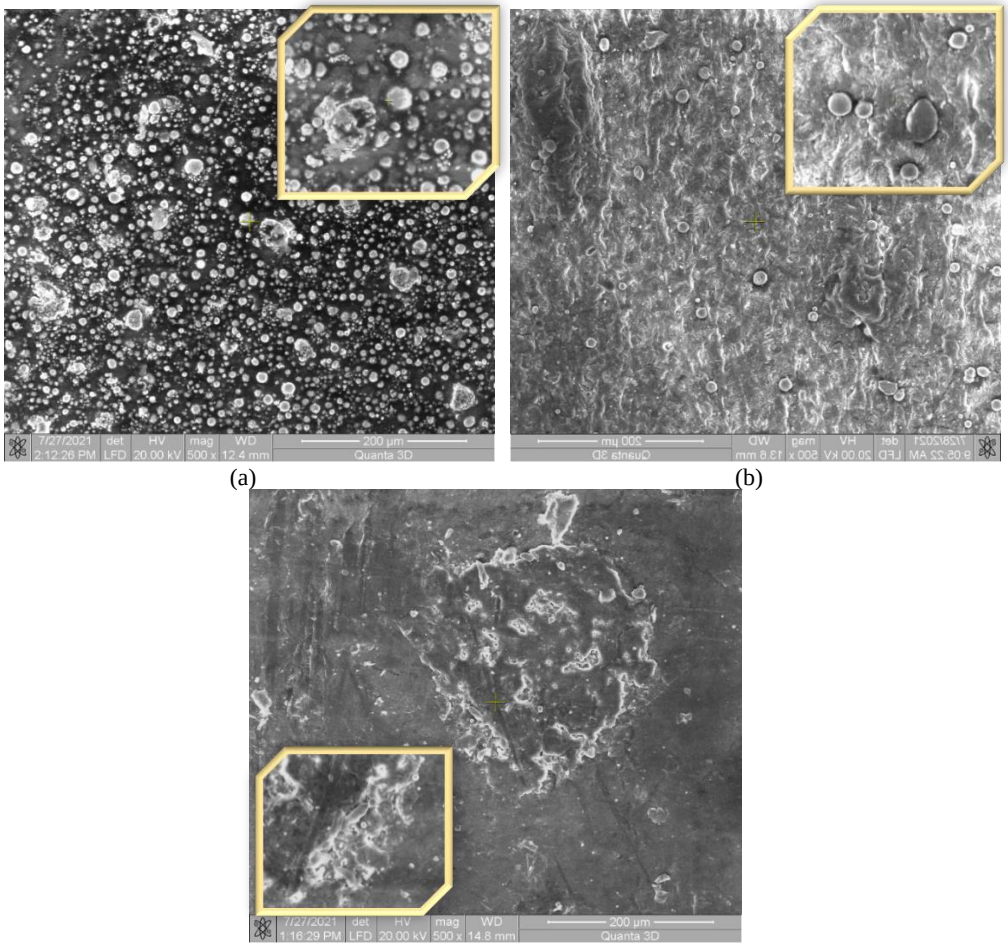

(a) (b)

(c)

Fig. 2. SEM analyses of the coated samples: (a) ZrO_2 $18TiO_2$ $10Y_2O_3$, (b) Cr_2O_3, (c) Cr_2O_3-$xSiO_2$-$yTiO_2$, magnification: x500 and x2000 for details.

3.3. XRD Analysis

The primary objective of the XRD study was to evaluate the structure of samples made of Arboblend V2 Nature and coated with ceramic micro-powders, as well as to identify potential crystal phases.

The phase diffractograms for the three samples with various ceramic coatings are depicted in Figure 3. Specific peaks reveal that two of the three samples (ZrO_2 $18TiO_2$ $10Y_2O_3$ and Cr_2O_3-$xSiO_2$-$yTiO_2$) have a crystalline structure, while the third (Cr_2O_3) has a semi-crystalline structure. The principal crystalline phases identified for the three coated samples are summarized in Table 2.

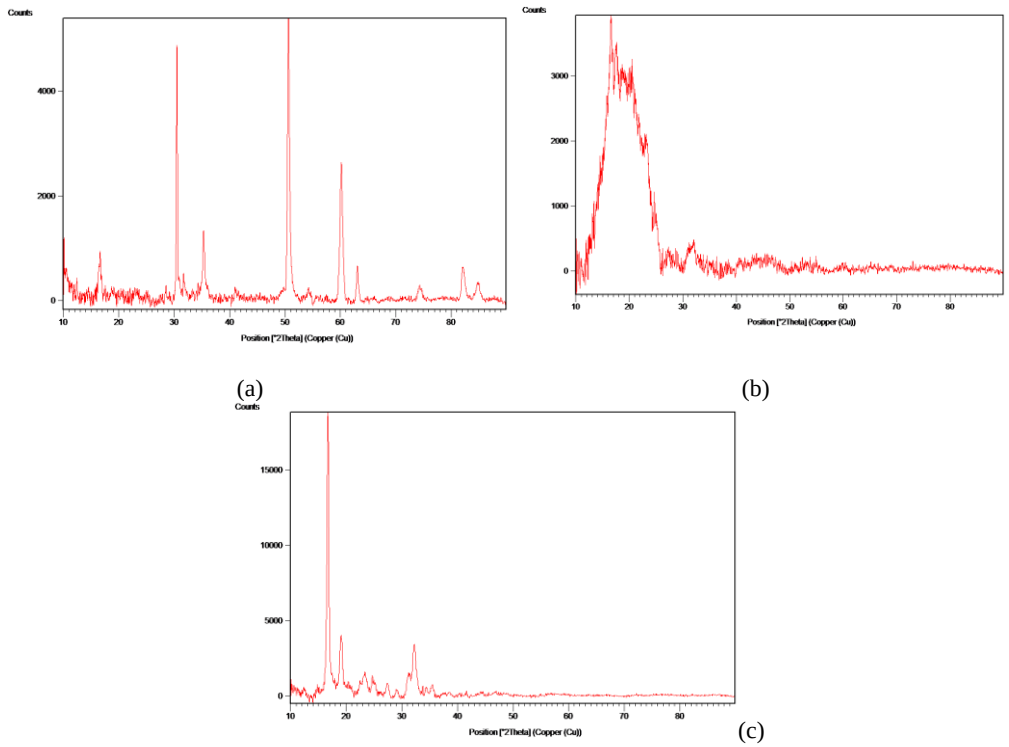

Fig. 3. XRD analyses of the coated samples: (a) ZrO_2 $18TiO_2$ $10Y_2O_3$, (b) Cr_2O_3, (c) Cr_2O_3-$xSiO_2$-$yTiO_2$

Table 2. Structure of the coted samples

Coating micro-powder	**Identified crystalline phases**	**Angle [°]**	**Reference**
ZrO_2 $18TiO_2$ $10Y_2O_3$	zirconium dioxide	31.14, 38.43, 60, 82 and 84.78	[30-32]
	titanium dioxide	27.43, 28.34, 63.02 and 74.41	[33, 34]
	yttrium oxide	43	[35]
Cr_2O_3	chromium oxide	24.25, 33.39, 35.88 and 54.61	[36–38]
	polylactic acid	16.73	[39, 40]
Cr_2O_3-$xSiO_2$-$yTiO_2$	chromium oxide	30.35, 31.70, 35.16, 50.48 and 54.12	[36–38, 41]
	titanium dioxide	27.33 and 32.13	[34, 35]
	silicon dioxide	22.5	[42]
	lignin or natural fibers	19.04	[33, 43]
	polylactic acid	16.73	[39, 40]

The fact that a polylactic acid compound was found in the structure of a Cr_2O_3-coated sample is not a coincidence. This is because the deposited layer is very thin (made up of small micro-particles), so the equipment is picking up one of the basic materials.

3.4. AFM Analysis

The samples were coated with three different types of ceramic powder (seven passes), and then analyzed with an atomic force microscope (AFM) in to identify any potential adhesion issues between the ceramic particles and the polymer substrate.

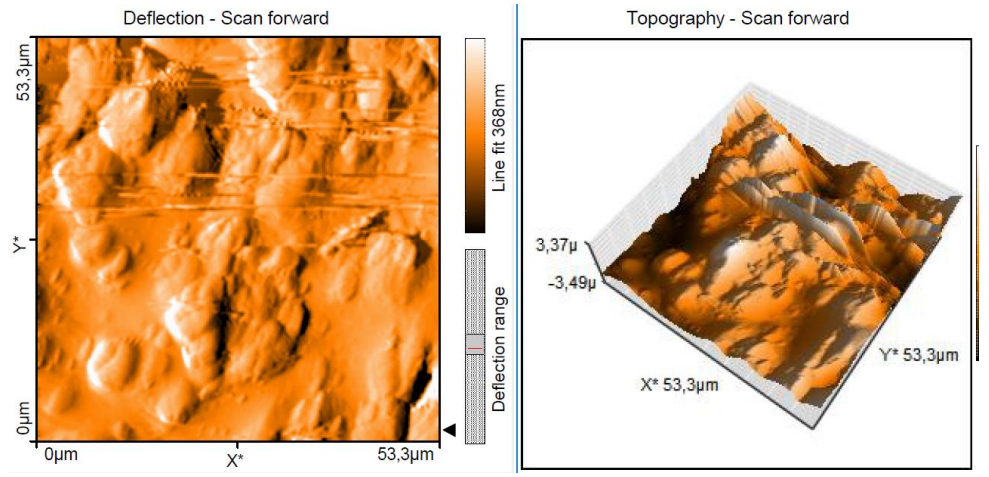

(a)

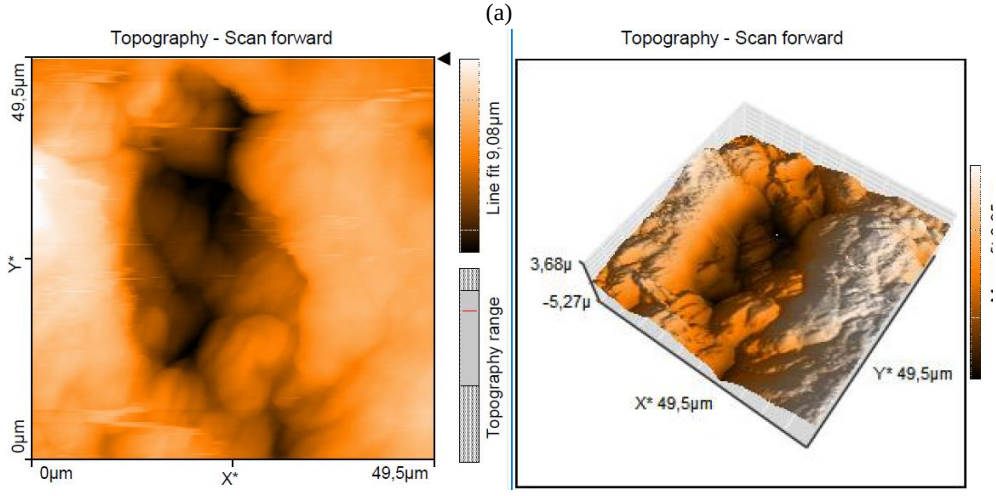

(b)

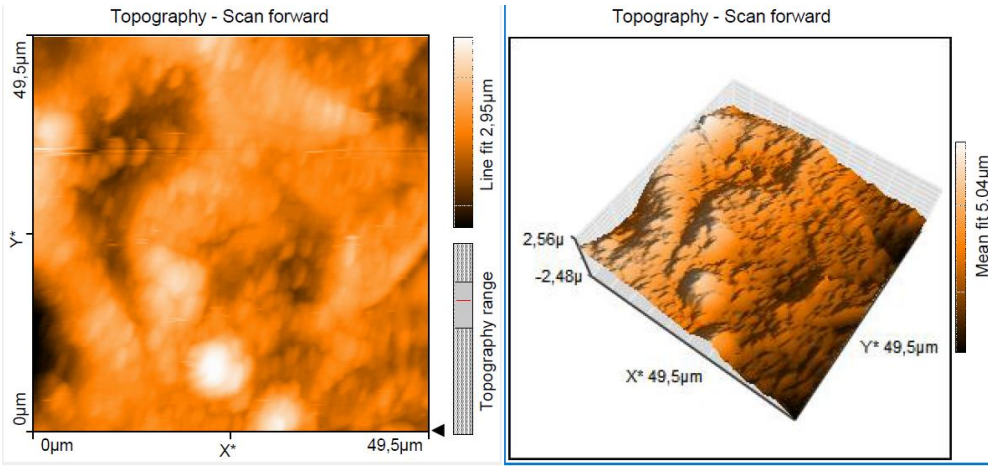

(c)

Fig. 4. AFM analyses of the coated samples: (a) Metco 143 (ZrO_2 $18TiO_2$ $10Y_2O_3$), (b) Amdry 6420 (Cr_2O_3), (c) Metco 136F (Cr_2O_3-$xSiO_2$-$yTiO_2$).

The surface topography of a Metco 143 (ZrO_2 $18TiO_2$ $10Y_2O_3$) coated Arboblend V2 Nature sample is displayed in Figure 4(a). By looking at the surface of the studied area ($49.5\mu m^2$), it is clear that the micro-particles are spread out evenly. Even though some of the micro particles were absorbed into the biopolymer mass, most of them maintained their spherical shape after coming into touch with the cold substrate. In chromium(III) oxide-coated samples, as shown in Figure 4(b), the smaller, spherical micro particles were embedded in the surface polymer structure, while the larger, rectangular micro particles were arranged in inhomogeneous patches.

Cr_2O_3-$xSiO_2$-$yTiO_2$, it is observed the relatively uniform deposition of micro-particles of different sizes and shapes on the surface of the sample. Therefore, the samples coated with Amdry 6420 and Metco 136F appear to exhibit poor micro-particle substrate adhesion compared to the sample coated with Metco 143. This may be because the chromium oxide that made contact with the polymer substrate did not adhere to it, most likely due to structural incompatibility but also to the process parameters.

One final sample, shown in Figure 4(c), coated with a chromium(III) oxide compound, Table 3 presents the surface roughness of the coated samples. It is observed the fact that the powder ZrO_2 $18TiO_2$ $10Y_2O_3$ has the lowest values of the roughness parameters, most likely due to the small dimensions of the ceramic micro-particles, which has been largely included. Therefore, it is considered that the adhesion of the ZrO_2 $18TiO_2$ $10Y_2O_3$ layer on the polymer substrate is a good one, because the micro ceramic particles created multiple bonds with the polymer substrate over the entire surface of the sample.

However, the other two coating types highlighted the existence of some portions where the particles actually did not stick to the substrate. This aspect is visible in

the case of Figure 4(b), which refers to the much different values of *Sa*, *Sq* parameters.

Table 3. Surface roughness parameters

Sample	Area (nm^2)	Sa (nm)	Sq (nm)	Sp (nm)	Ra in line (nm)
Metco 143 ZrO_2 18TiO_2 10Y_2O_3	2.87	104.51	119.11	1150.4	54.567
Amdry 6420 Cr_2O_3	2.47	1578.5	1915.3	4746.7	1308.7
Metco 136F Cr_2O_3-xSiO_2-yTiO_2	2.47	323.32	419.74	1582.8	485.69

where: *Sa* (arithmetical mean height) - average surface roughness; *Sq* (root mean square height) - Standard deviation of the height distribution, or RMS surface roughness; *Sp* (Maximum peak height) - Height between the highest peak and the mean plane; Ra - line roughness

4. Conclusions

The coatings were developed to enhance the mechanical, tribological, and thermal properties of the samples (wear, hardness, and increase in thermal resistance), making them better for applications that need to work in harsh conditions, like the automotive industry. The following happened after the sample was covered with ceramic microlayers:

- The thermal analysis highlighted the thermal stability of the coated sample, its structure being no altered.
- In terms of how uniform the coatings are, the SEM surface analysis showed that the composite powder made from zirconium oxide did a good job of incorporating micro-particles in a uniform way. The other two ceramic micro-powders didn't stick well to the polymer matrix because they were used at temperatures lower than the melting point, which is around 2435 °C.
- XRD tests showed that there were layers of micro-ceramics. Their crystalline or semi-crystalline structure makes them hard, so they can be used in situations where this is needed.
- The AFM analyze highlighted the good adhesion between the ceramic particles and the polymer substrate especially for the sample coated with Zirconia–Titania–Yttria Composite Powder.

According to the results obtained for the adhesion of the ceramic layers on the polymer surface, the samples demonstrated strong chemical bonds at the interface between the thin layers and the Arboblend V2 Nature bio-based polymer. As a result, these coated materials are suitable for industrial applications requiring high surface hardness and thermal resistance. They can also successfully replace non-biodegradable polymeric materials used in a variety of applications, including those in the automotive and electronics industries (telephone covers, housings, worm wheels, car wiper system, etc.).

References

[1] Lampe T., Eisenberg S., Cabeo E.R., *Plasma surface engineering in the automotive industry—trends and future prospectives*, Surf. Coat. Technol., **174**, 2003, p. 1–7.
[2] Wang Y., Jiang S., Wang M.D., Wang S.H., Xiao T.D., Strutt P.R., *Abrasive wear characteristics of plasma sprayed nanostructured alumina/titania coatings*, Wear, **237**, 2000, p. 176–185.
[3] Choi J.W., Hwang G.H., Han W.K., Lee W.H., Kang S.G., *Effect of Cu on the surface hardness of Ni–B coating for the strengthening of the Cu surfac*e, Met. Mater. Int., **13**, (2007), p. 403–409.
[4] Choe H.C., Ko Y.M., *Interface activation and surface characteristics of Ti/TiN/HA coated sintered stainless steels*, Met. Mater. Int., **12**, 2006, 31–37.
[5] Petrovicova E., Schadler L.S., *Thermal spraying of polymers*, Int. Mater. Rev., **47**, 2002, p. 169–190, https://doi.org/10.1179/095066002225006566.
[6] Gonzalez R., Ashrafizadeh H., Lopera A., Mertiny P., McDonald A., *A review of thermal spray metallization of polymer-based structures*, J. Therm. Spray. Technol., **25**, 2016, p. 897–919.
[7] Shacham-Diamand Y., Osaka T., Okinaka Y., Sugiyama A., Dubin V., *30 Years of electroless plating for semiconductor and polymer micro-system*s, Microelectron. Eng., **132**, 2015, p. 35–45.
[8] Ghosh S., *Electroless copper deposition: a critical review*, Thin Solid Films, **669**, 2019, 641–658.
[9] Mavukkandy M.O., McBride S.A., Warsinger D.M., Dizge N., Hasan S.W., Arafat H. A., *Thin film deposition techniques for polymeric membranes – a r*eview, J. Memb. Sci., **610**, 2020, 118258.
[10] Ferreira A.A., Silva F.J.G., Pinto A.G., Sousa V.F.C., *Characterization of thin chromium coatings produced by PVD sputtering for optical applications*, Coatings, **11**, 2021, p. 1–20.
[11] Gariboldi E., Rovatti L., Lecis N., Mondora L., Mondora G.A., *Tribological and mechanical behaviour of Cr3C2–NiCr thermally sprayed coatings after prolonged aging*, Surf. Coat. Technol., **305**, 2016, p. 83–92.
[12] Tsui Y.C., Clyne T.W., A*n analytical model for predicting residual stresses in progressively deposited coatings Part 1: Planar geometry*, Thin Solid Films, **306**, 1997, p. 23–33.
[13] Heli Koivuluoto, *Review of Thermally Sprayed Polymer Coatings*, J Therm Spray Tech, https://doi.org/10.1007/s11666-022-01404-1.
[14] Marguta A., Nedelcu D., Mazurchevici S.-N., *Thermal behavior of coated bio-polymers*, International Journal of Modern Manufacturing Technologies, **XIV,** 3, 2022, p. 146-151, https://doi.org/ 10.54684/ijmmt.2022.14.3.146.
[15] Divine S., Chun-Wei Y., Ian L., *Mechanical durability of engineered superhydrophobic surfaces for anti-corrosion*, Coatings, **8**, 2018, 162.
[16] Ulaeto S., Rajan R., Pancrecious J., Rajan T., Pai B., *Developments in smart anticorrosive coatings with multifunctional characteristics*, Prog. Org. Coat., **111**, 2017, p. 294–314.
[17] Asri N., Husaini T., Sulong A., Majlan E., Daud W., *Coating of stainless steel and titanium bipolar plates for anticorrosion in PEMFC: A review*, Int. J. Hydrogen Energy, **42**, 2017, p. 9135–9148.
[18] Fengjuan X., Cheng Q., Mingyang G., Junzhong W., Xinrui Y., Hongli L., Lin Y., *Anticorrosive durability of zinc-based waterborne coatings enhanced by highly dispersed and conductive polyaniline/graphene oxide composite*, Prog. Org. Coat., **125**, 2018, p. 79–88.
[19] Sorensen P., Kiil S., Dam-Johansen K., Weinell C., *Anticorrosive coatings: A review*, J. Coat. Technol. Res., **6**, 2009, p. 135–176.
[20] TECNARO–The Biopolymer Company. Available online: https://www.tecnaro.de/en/ (20/08/2022).
[21] Mazurchevici S.-N., Mazurchevici A.-D., Nedelcu D., *Dynamical mechanical and thermal analyses of biodegradable raw materials for additive manufacturing*, Materials, **13**, 2020, p. 1819.
[22] Mazurchevici S.-N., Motas J.G., Diaconu M., Lisa G., Lohan N.M., Glod M., Nedelcu D., *Nanocomposite biopolymer arboblend V2 nature AgNPs*, Polymers, **13**, 2021, p. 2932.
[23] Nedelcu D., Marguta A., Mazurchevici S., Munteanu C., Istrate B., *Micro-structural and morphological analyses of coated 'liquid wood' samples by ceramic particles*, Mater. Res. Express, **6**, 2019, 085326.
[24] Broitman E., Nedelcu D., Mazurchevici S., Glenat H., Grillo S., *Tribological and nanomechanical behavior of liquid wood*, J. Tribol., **141**, 2019, 022001.

[25] Nedelcu D., Santo L., Santo A.G., Plavanescu Mazurchevici S., *Mechanical behaviour evaluation of arboform material samples by bending deflection test*, Mater. Plast., 52, 2015, 423–426.
[26] Oerlikon Metco–Materials and Surface Solutions. Available online: https://www.oerlikon.com/metco/en/ (12/06/2020).
[27] Mazurchevici S.-N., Marguta A., Istrate B., Benchea M., Boca M., Nedelcu D., *Improvements of Arboblend V2 Nature Characteristics through Depositing Thin Ceramic Layers*, Polymers, **13**, 2021, 3765. https://doi.org/10.3390/polym13213765.
[28] Brebu M., Vasile C., *Thermal degradation of lignin—A review*, Cell Chem. Technol., **44**, 2010, p. 353–363.
[29] Wagner M., *Thermal analysis in practice, fundamental aspects*, In Thermal Analysis in Practice; Wagner, M., Ed.; Hanser: München, Germany, 2018; pp. 1–9. ISBN 9781569906439.
[30] Istrate B., Rau J.V., Munteanu C., Antoniac I.V., Saceleanu S., *Properties and in vitro assessment of ZrO2-based coatings obtained by atmospheric plasma jet spraying on biodegradable Mg-Ca and Mg-Ca-Zr alloys*, Ceram. Int., **46**, 2020, p. 15897–15906.
[31] Wu C.-S., *Analysis of mechanical, thermal, and morphological behavior of polycaprolactone/wood flour blends*, J. Appl. Polym. Sci., **94**, 2004**,** p. 1000–1006.
[32] Onkar M., Savita R., *Monoclinic zirconium oxide nanostructures having tunable band gap synthesized under extremely non-equilibrium plasma cond*itions, Proceedings, **3**, 2019, 10.
[33] Sagadevan S., Jiban P., Isha D., *Hydrothermal synthesis of zirconium oxide nanoparticles and its characterization*, J. Mater. Sci. Mater. Electron., **27**, 2016, 5622–5627.
[34] Suning L., Qian W., Tao C., Zhihua Z., Ying W., Jiajun F., *Study on cerium-doped nano-TiO2 coatings for corrosion protection of 316 L stainless steel*, Nanoscale Res. Lett., **7**, 2012, p. 227.
[35] Vorrada L., Natnapin J., Thirawich C., Achanai B., *The photocatalytic reduction of hexavalent chromiumby controllable mesoporous anatase TiO2 nanoparticles*, Adv. Mater. Sci. Eng., 2014, 348427.
[36] Fatemeh T., Alireza S., Hossein M., *Synthesis of Cr2O3/TiO2 nanocomposite and its application as the blocking layer in solar cells*, J. Environ. Anal. Chem., **5**, 2018, 1000231.
[37] Bhagyashri K., Mahesh N., Garadkar K.M., Rahul B.M., Kiran Kumar K.S., Balu D.A., Shivaji T., *Ionic liquid assisted synthesis of chromium oxide (Cr2O3) nanoparticles and their application in glucose sensing*, J. Mater. Sci. Mater. Electron., 30, 2019, 13984–13993.
[38] Sone B.T., Manikandan E., Gurib-Fakim A., Maaza M., *Single-phase _-Cr2O3 nanoparticles' green synthesis using Callistemon viminalis' red flower extract*, Green Chem. Lett. Rev., 9, 2016, p. 85–90.
[39] Benwood C., Anstey A., Andrzejewski J., Misra M., Mohanty A.K., *Improving the impact strength and heat resistance of 3d printed models: Structure, property, and processing correlationships during fused deposition modeling (FDM) of Poly(Lactic Acid)*, ACS Omega, 3, 2018, p. 4400–4411.
[40] Teixeira E.d.M., Campos A.d., Marconcini J.M., Bondancia T.J., Woo D., Klamczynski A., Mattosoa L.H.C., Glenn G.M., S*tarch/fiber/poly(lactic acid) foam and compressed foam composites*, RSC Adv., 4, 2014, p. 6616–6623.
[41] Gupta A.K., Mohanty S., Nayak S.K., *Preparation and characterization of lignin nanofibre by electrospinnig technique*, Int. J. Sci. Eng. Appl. Sci., **1**, 2015, 184–190, ISSN:2395-3470.
[42] Adnan A., Shahid A., Murtaza S., Shahid M.R., Shahzad N., Saadat A.S., *Structural and magnetic phase transition of sol–gel-synthesized Cr2O3 and MnCr2O4 nanoparticles*, J. Sol-Gel Sci. Technol, **80**, 2016, p. 96–102.
[43] Tamrakar R.K., Upadhyay K., Bisen D.P., *Gamma ray induced thermoluminescence studies of yttrium (III) oxide nanopowders doped with gadolinium*, J. Radiat. Res. Appl. Sci., **7**, 2014, p. 526–531.